Electronic Supplementary Material (ESI) for Physical Chemistry Chemical Physics.
This journal is © the Owner Societies 2016

Supplementary Information

Visible Luminescent lanthanide ions and large π-conjugate ligand system shake hands

Y. Kitagawa,[a] R. Ohno,[b] T. Nakanishi,[a] K. Fushimi,[a] and Y. Hasegawa[a]

Affiliations

[a]Faculty of Engineering, Hokkaido University, N13 W8, Kita-ku, Sapporo, Hokkaido 060-8628, Japan

[b]Graduate School of Chemical Sciences and Engineering, Hokkaido University, N13 W8, Kita-ku, Sapporo, Hokkaido 060-8628, Japan

Contact Information

Tel/Fax: +81 11 706 7114

[*]E-mail: y-kitagawa@eng.hokudai.ac.jp, hasegaway@eng.hokudai.ac.jp

S1. Synthetic scheme and chemical structures

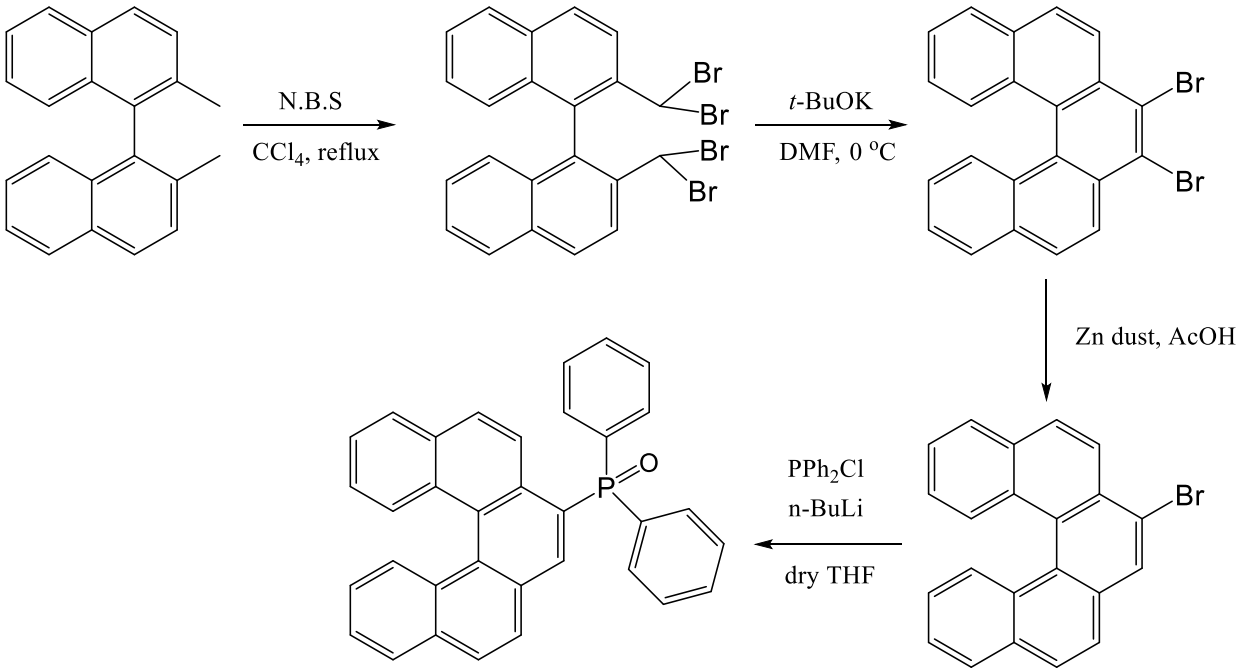

Figure S1. Synthetic scheme of ligand.

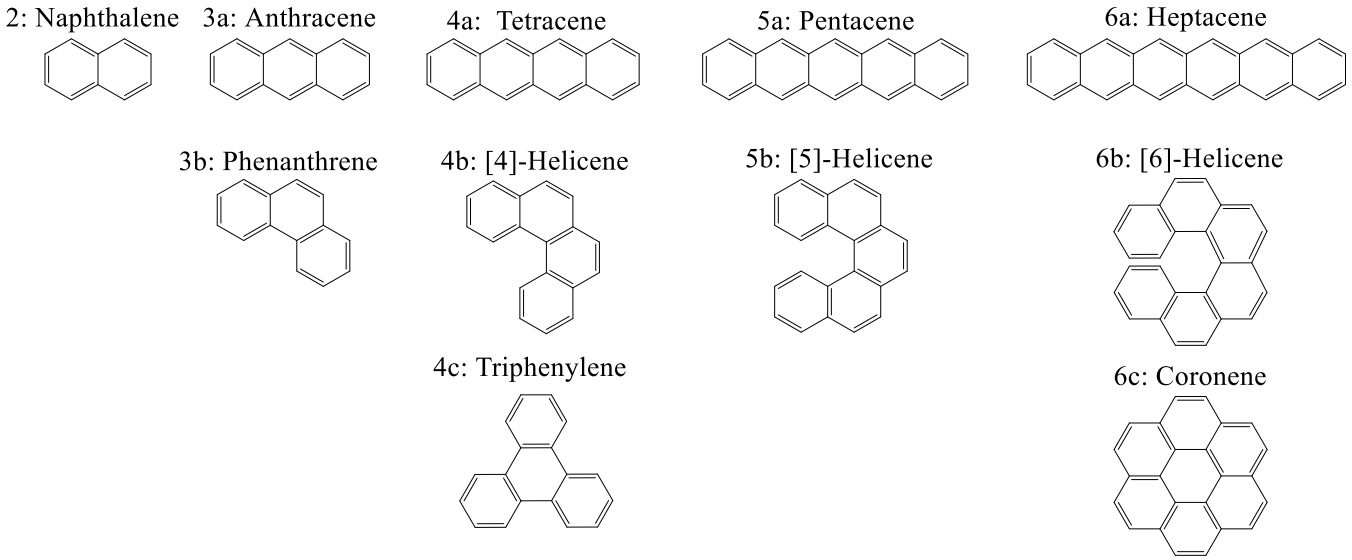

Figure S2. Chemical Structures of aromatic compounds.

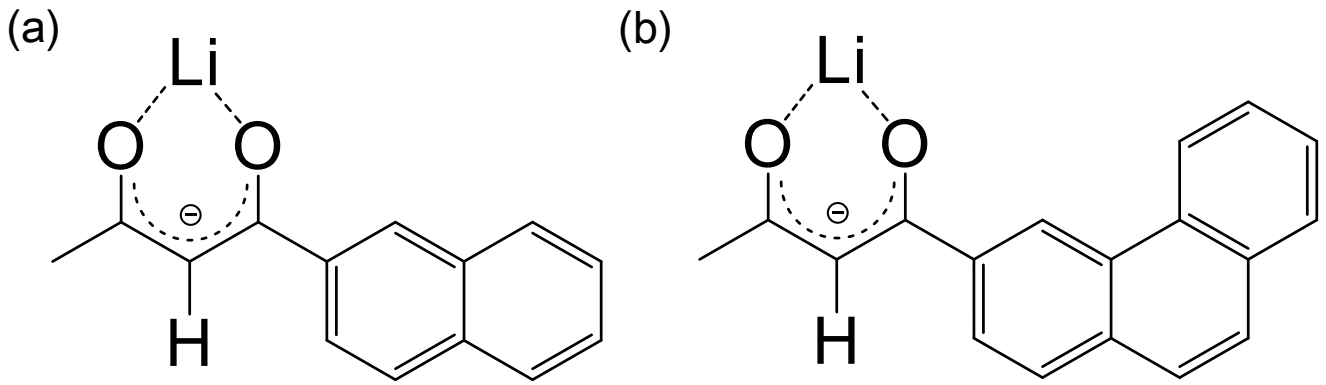

Figure S3. Chemical Structures of hetero-π-conjugated molecules (a: Li(nbd) (nbd = 1-(2-naphthyl)-1,3-butanedione), b: Li(pbd) (pbd = 1-(3-phenanthrenyl)-1,3-butanedione)).

S2. Synthesis schemes

7-bromo-[5]-helicene and $Eu(hfa)_3(H_2O)_2$ were synthesized according to the previous reports.[5-7, 49-50]

2,2-bis(dibromomethyl)-1,1-binaphthyl[49]

(S)-2,2'-Dimethyl-1,1'-binaphthyl (0.51g, 1.8 mmol) was dissolved in carbon tetrachloride (10 ml), and then N-bromosuccinimide (3.6 g, 20 mmol) was added to the solution. The mixture was refluxed for 40 h under Ar. After reaction, the reactant was filtrated in order to remove the excess of N-bromosuccinimide, and the filtrate was washed with NaCl aq. and distilled H_2O. The organic layer was separated and dried with $MgSO_4$, and the solvent was evaporated. The compounds were separated by silica gel chromatography (dichloromethane: hexane = 2 : 8). 2,2'-bis(dibromomethyl)-1,1'-binaphthyl (0.81 g, 1.3 mmol) was obtained (Yield: 75 %).

^{1}H NMR ($CDCl_3$, 400 MHz, TMS, ppm): 6.21 (s, 2H); 6.98 (d, 2H, *J* = 8.4 Hz); 7.24-7.35 (m, 2H); 7.49-7.58 (m, 2H); 7.96 (d, 2H, *J* = 8.0 Hz); 8.15 (d, 2H, *J* = 8.8 Hz); 8.24 (d, 2H, *J* = 8.8 Hz). **MS** (EI, 2000 V): *m/z* calcd for $C_{22}H_{14}Br_4$ $[M]^+$ = 597.78; found: 597.84.

7,8-dibromo-[5]-helicene[49]

2,2'-bis(dibromomethyl)-1,1'-binaphthyl (0.81 g, 1.3 mmol) was dissolved in DMF (10 ml). This solution was cooled at 273 K. After the solution was stirred for 5 h, the potassium *t*-butoxide (2.6 g, 23 mmol) was

added slowly. The sample color change from yellow to brown, and the sample was stirred for 15 min. And then, the reactant solution was added to HCl (0.12 M, 100ml), the pale yellow powder was obtained. In addition, HCl (6 M) was added slowly to the reactant solution until pH 1, the reactant was filtrated, and washed with methanol. The 7,8-dibromo-[5]-helicene (0.54 g, 1.2 mmol) was obtained (Yield: 92 %). **^{1}H NMR** ($CDCl_3$, 400 MHz, TMS, ppm): 7.19-7.29 (m, 2H); 7.50-7.58 (m, 2H); 7.91-8.03 (m, 4H); 8.24 (d, 2H, *J* = 8.8 Hz); 8.46 (d, 2H, *J* = 9.2 Hz); **MS** (EI, 1900 V): *m/z* calcd for $C_{22}H_{12}Br_2$ $[M]^+$ = 435.93; found: 435.96.

7-bromo-[5]-helicene[49]

7,8-dibromo-[5]-helicene (0.53g, 1.2 mmol) and zinc dust (0.43 g, 6.6 mmol) was dissolved into acetate (40 ml). The mixture was refluxed for 5h at 130 ^{o}C. After the reactions, the reaction was filtrated in order to remove the zinc dust. The filtrate was cooled, and flocculating crystal was obtained. This crystal was washed with methanol. 7-bromo-[5]-helicene (0.37 g, 1.0 mmol) was obtained (Yield: 85 %). **^{1}H NMR** ($CDCl_3$, 400 MHz, TMS, ppm): 7.20-7.32 (m, 2H); 7.47-7.60 (m, 2H); 7.78 (d, 1H, *J* = 8.8 Hz); 7.90-8.04 (m, 4H); 8.19 (s, 1H); 8.32-8.40 (m, 2H); 8.43 (d, 1H, *J* = 8.8 Hz). **MS** (EI, 2100 V): *m/z* calcd for $C_{22}H_{13}Br$ $[M]^+$ = 356.02; found: 356.07.

$Eu(hfa)_3(H_2O)_2$[5-7, 50]

$Eu(hfa)_3(H_2O)_2$ was prepared according to the previous method.[5-7, 50] **Elemental analysis** calcd for $C_{15}H_7EuF_{18}O_8$: C 22.27, H 0.87; found: C 22.12, H 1.01.

S3. Molecular orbitals

First, the optimum structures of aromatic compounds (Figure S2) were calculated by the DFT method (B3LYP/6-31G*, Gaussian 03).[29-30] The optimum structures and molecular orbitals are shown in Figures S4-S15. The LUMO+1, LUMO, HOMO, and HOMO-1 orbital energies for acene are summarized in Figure S20a. By the extension of π-conjugation, the HOMO and LUMO energy levels become higher and lower respectively, which induces a small HOMO-LUMO gap. On the other hand, in the case of the extension of helical π-conjugation, the HOMO and LUMO energy levels become slightly higher and lower respectively (Figure S20b) and show a relatively high T_1 energy ([4]-helicene: T_1 = 19980 cm^{-1}, [5]-helicene: T_1 = 19700 cm^{-1}, [6]-helicene: T_1 = 19060 cm^{-1})[32]. In case of the extension of planar π-conjugation, the HOMO and LUMO energy levels are almost unchanged for triphenylene and become higher and lower, respectively, for coronene (Figure S20c). These high-symmetry structures induce degenerate HOMO and LUMO energy levels (Figures S10 and S15). The T_1 states formed by strong interactions between the HOMO−1→LUMO and the HOMO→LUMO+1 electronic configurations show high energy levels (triphenylene: T_1 = 23580 cm^{-1}, coronene: T_1 = 19400 cm^{-1})[27]. In addition, DFT calculations (B3LYP/6-31G*, Gaussian 03) were performed on hetero-π-conjugated molecules bonded to a lithium ion (Figure S3).[48] The optimum structures and molecular orbitals are shown in Figures S16, S17, and S19.

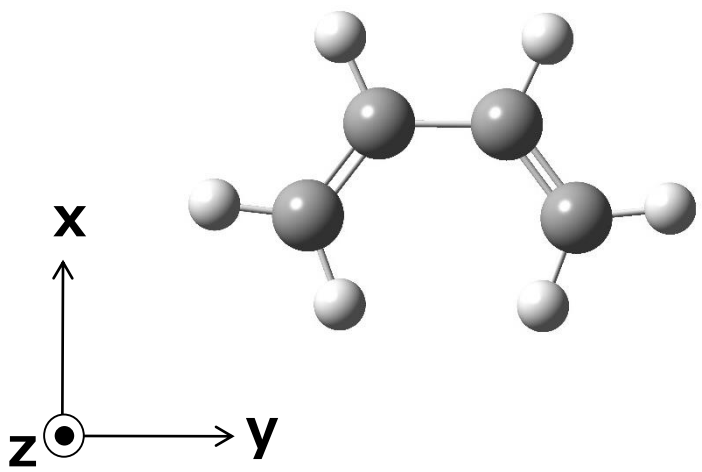

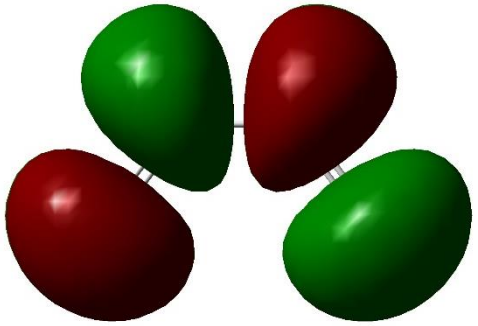

LUMO+1(2.62 eV)

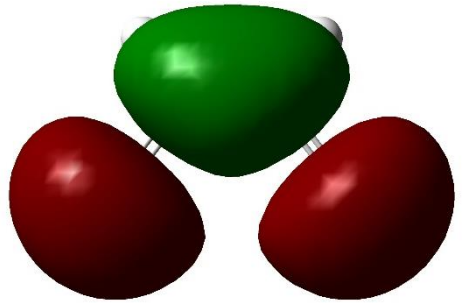

LUMO(-0.82 eV)

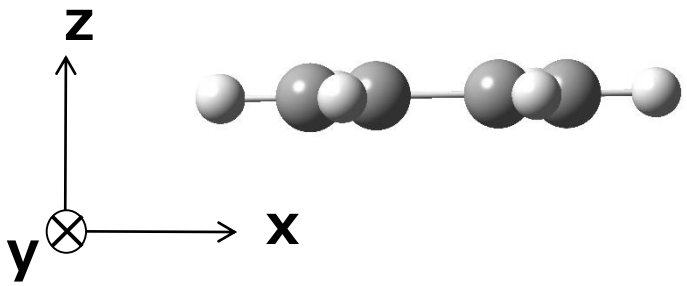

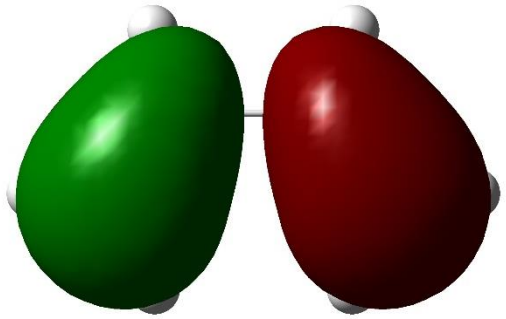

HOMO(-6.19 eV)

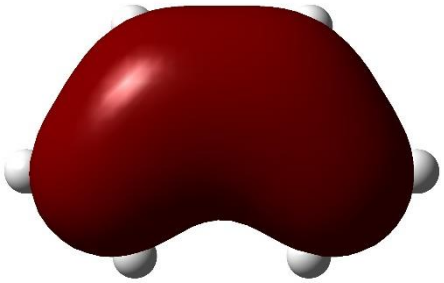

HOMO-1(-8.63 eV)

Figure S4 Molecular orbitals of butadiene.

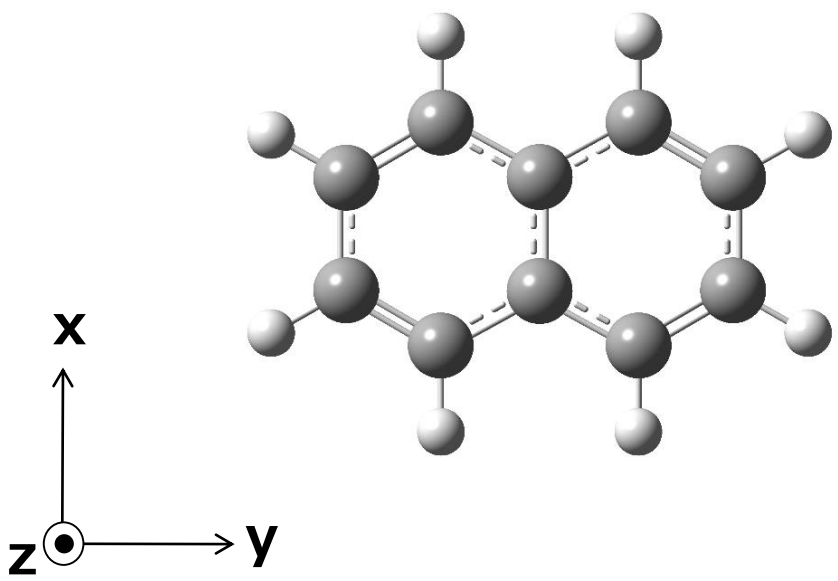

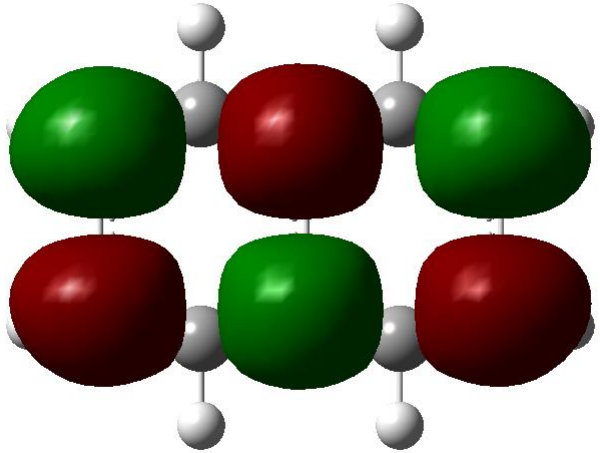

LUMO+1(-0.15 eV)

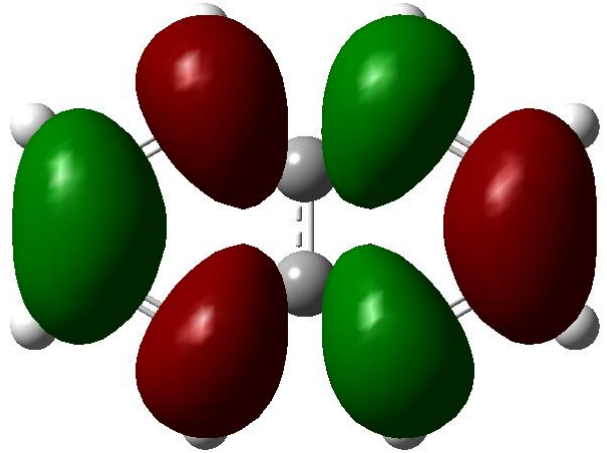

LUMO(-0.96 eV)

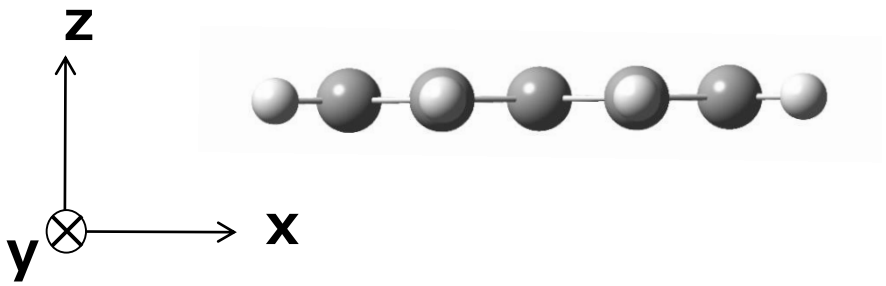

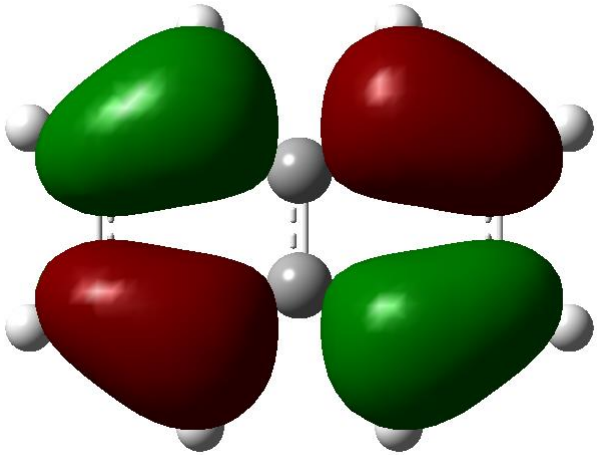

HOMO(-5.79 eV)

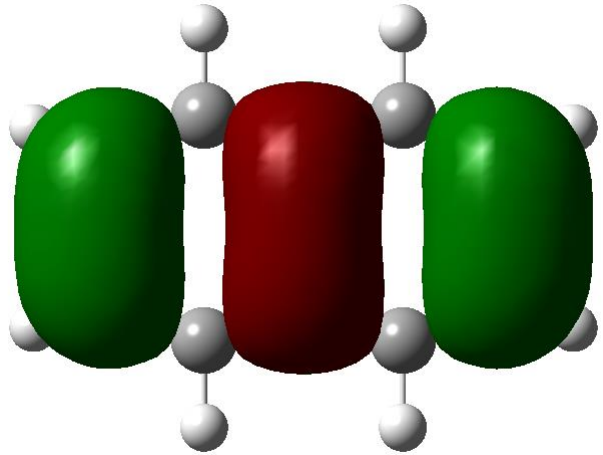

HOMO-1(-6.54 eV)

Figure S5 Molecular orbitals of naphthalene (2).

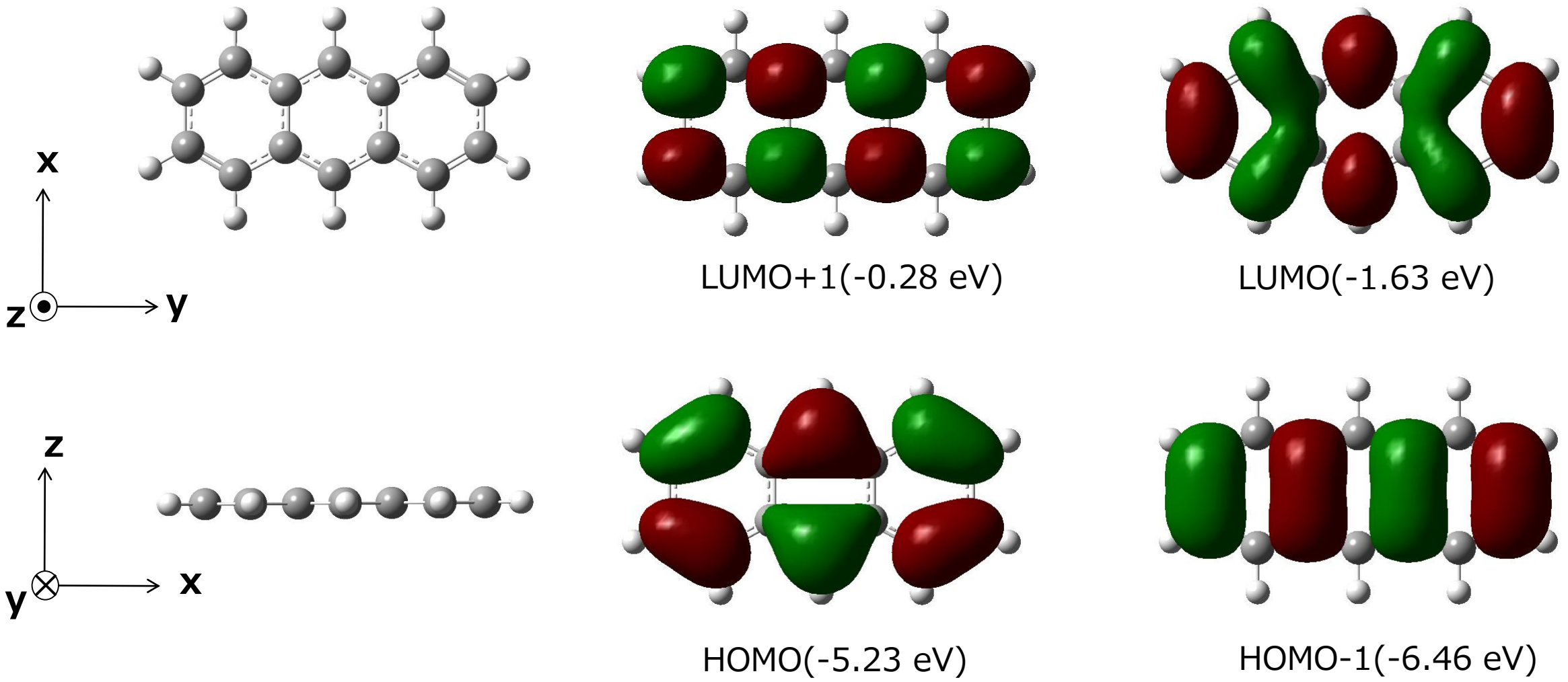

Figure S6 Molecular orbitals of anthracene (3a).

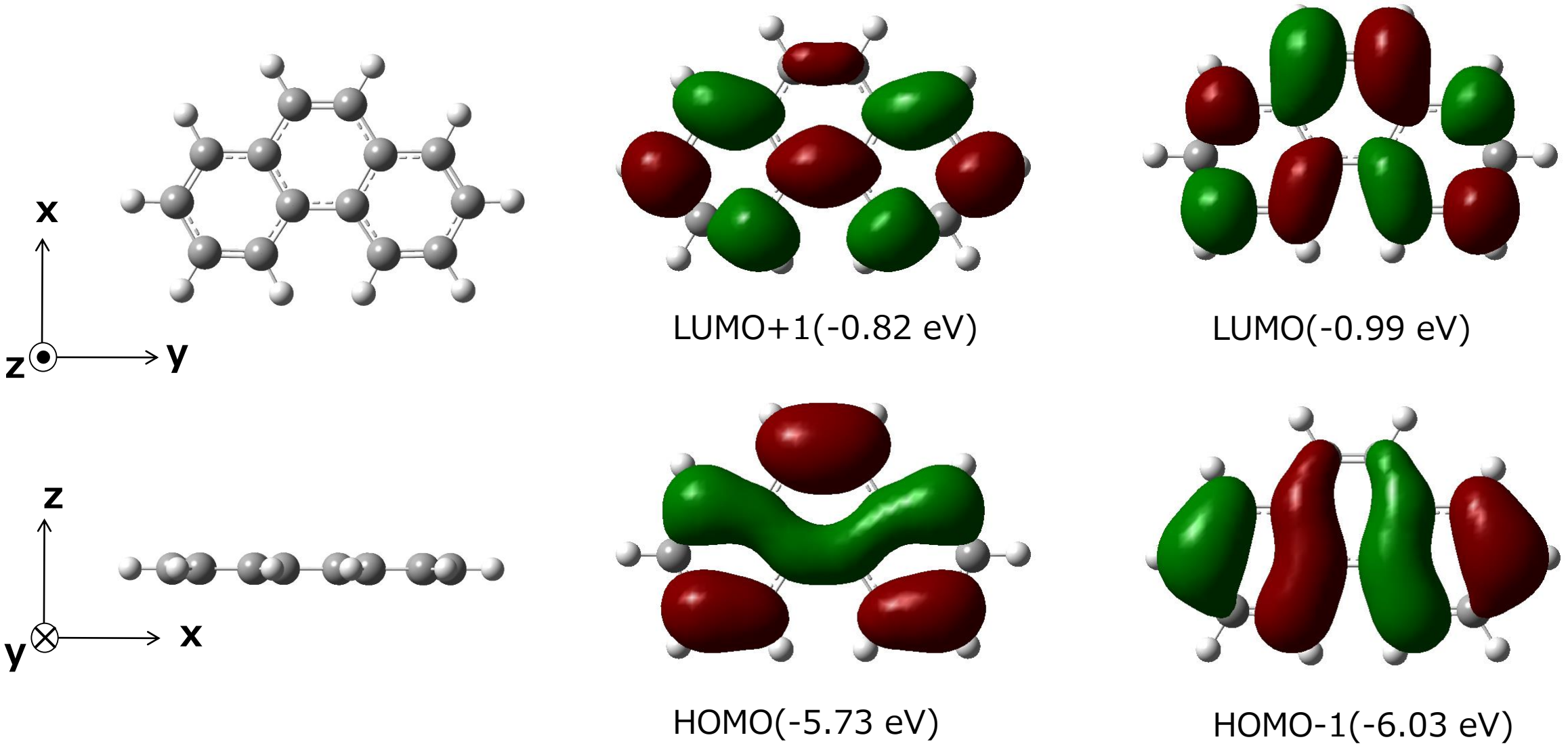

Figure S7 Molecular orbitals of phenanthrene (3b).

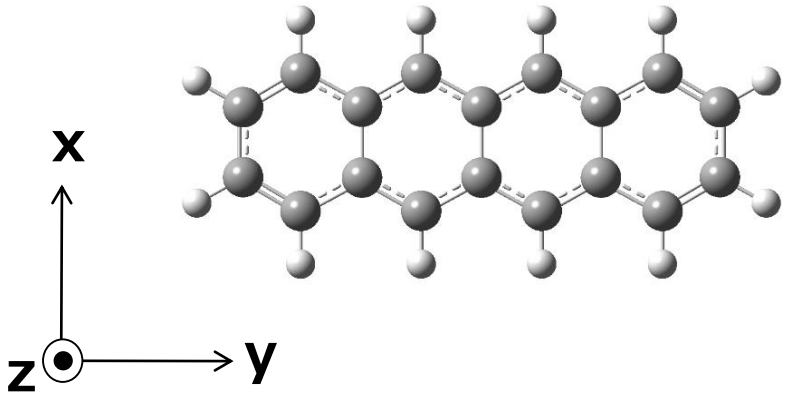

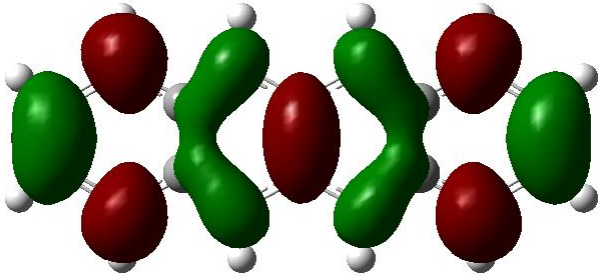

LUMO+1(-0.42 eV)

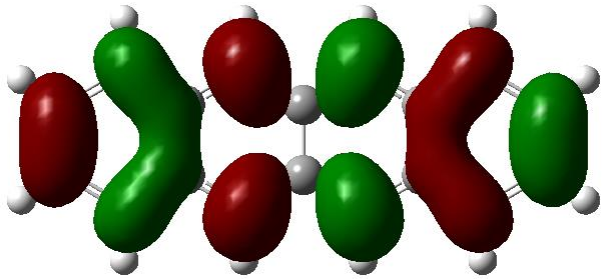

LUMO(-2.08 eV)

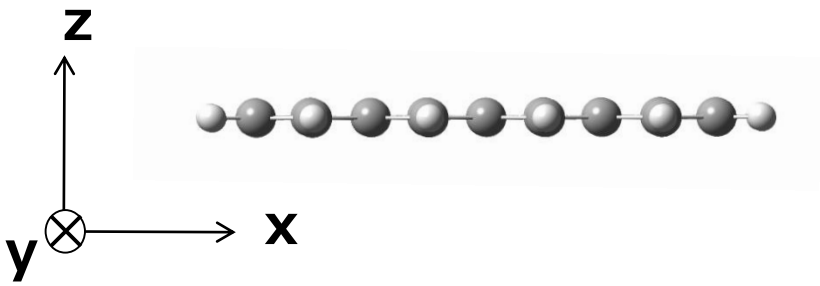

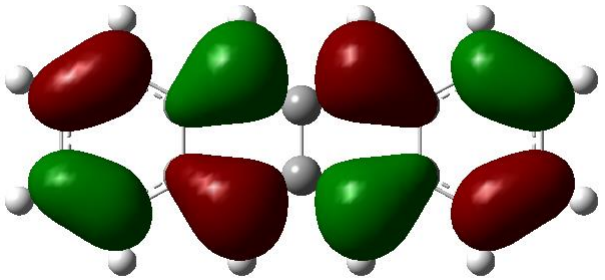

HOMO(-4.86 eV)

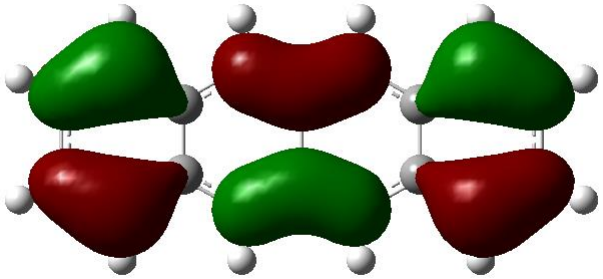

HOMO-1(-6.33 eV)

Figure S8 Molecular orbitals of tetracene (4a).

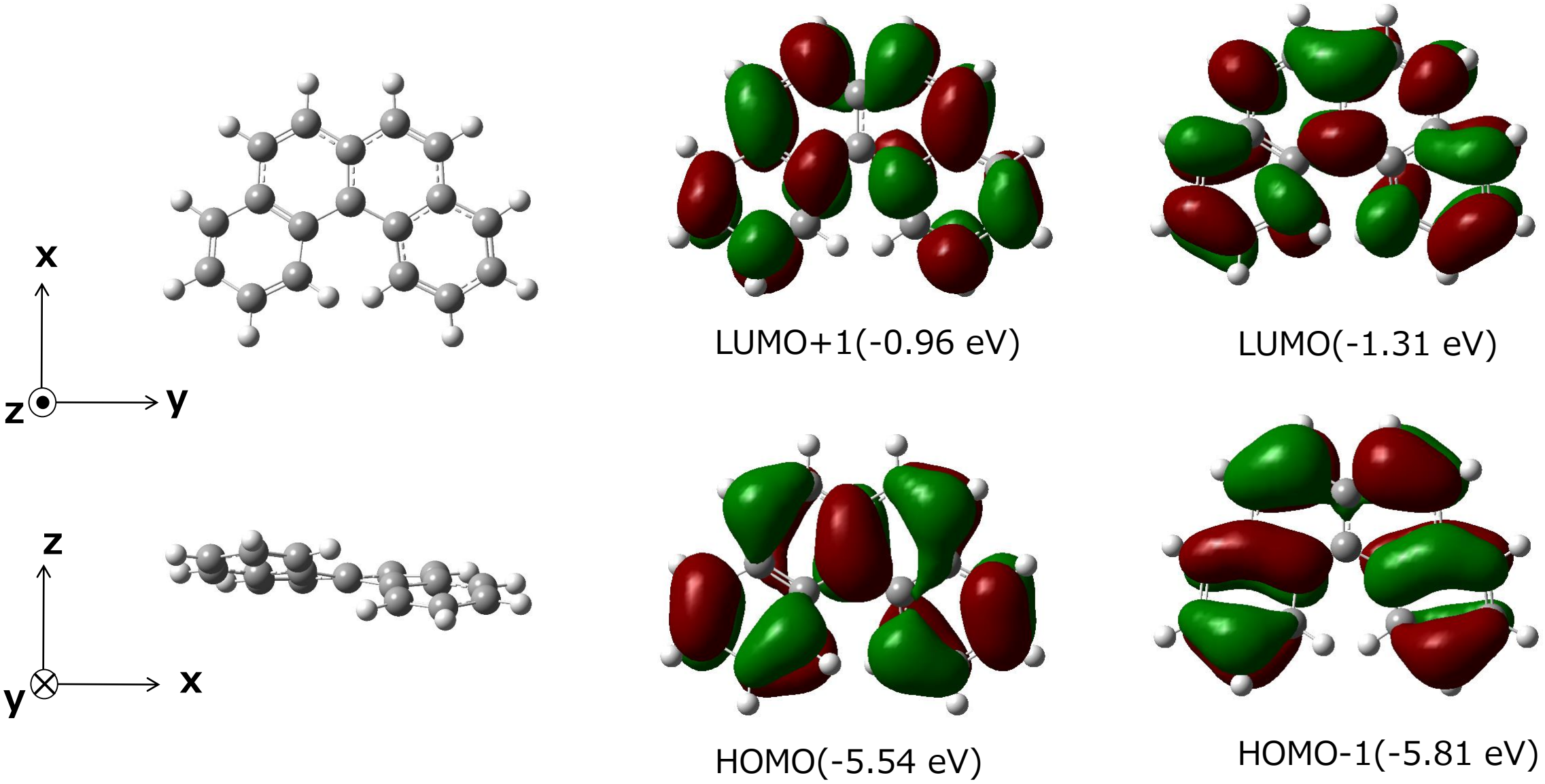

Figure S9 Molecular orbitals of [4]-helicene (4b).

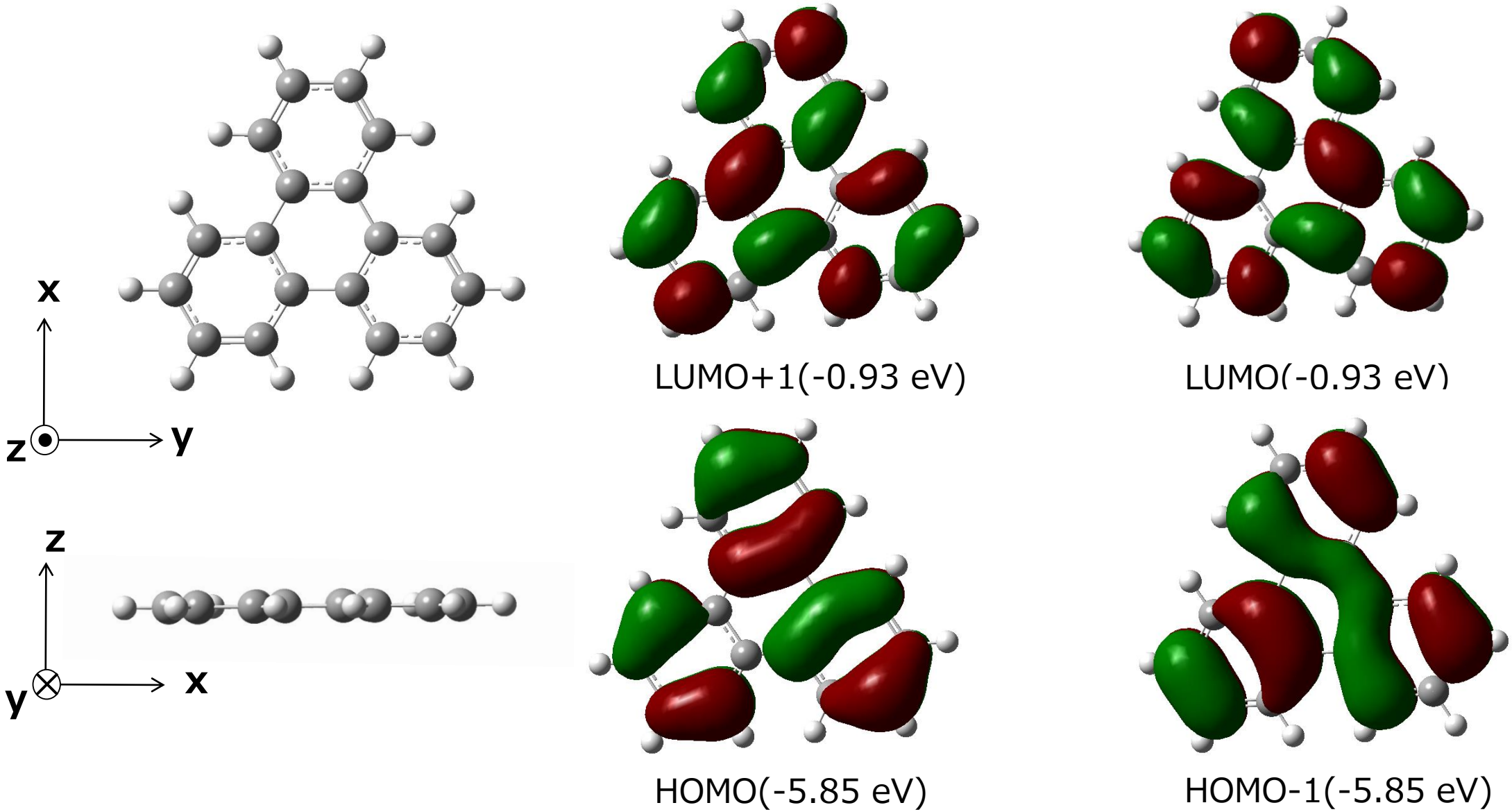

Figure S10 Molecular orbitals of triphenylene (4c).

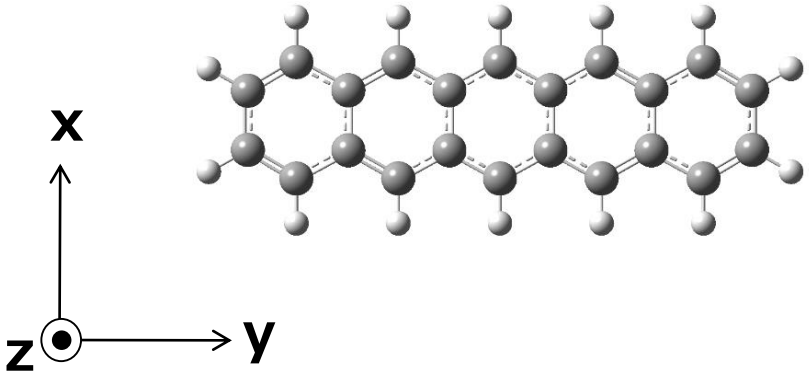

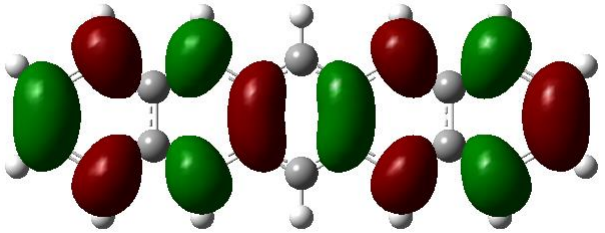

LUMO+1(-0.94 eV)

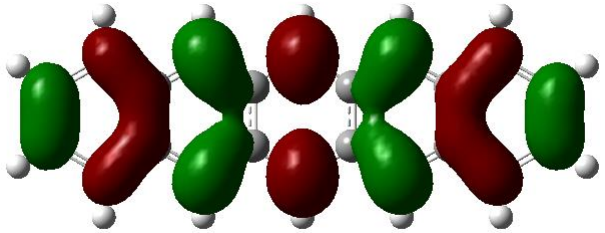

LUMO(-2.39 eV)

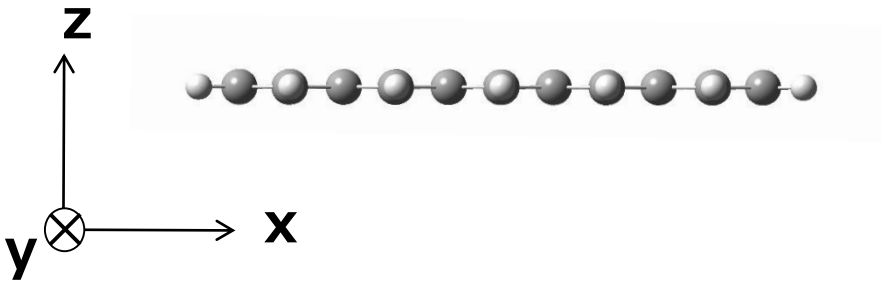

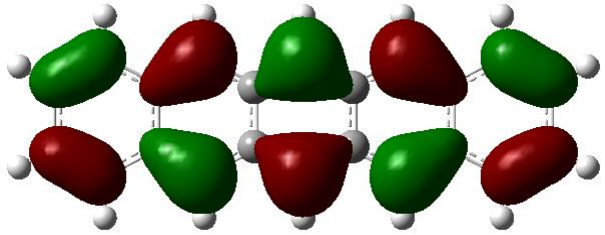

HOMO(-4.60 eV)

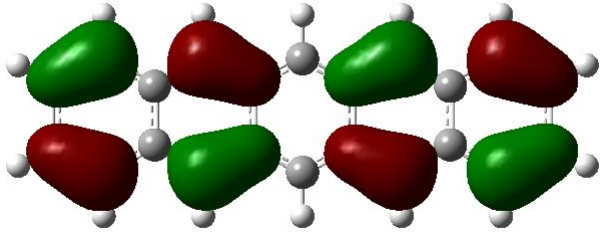

HOMO-1(-5.88 eV)

Figure S11 Molecular orbitals of pentacene (5a).

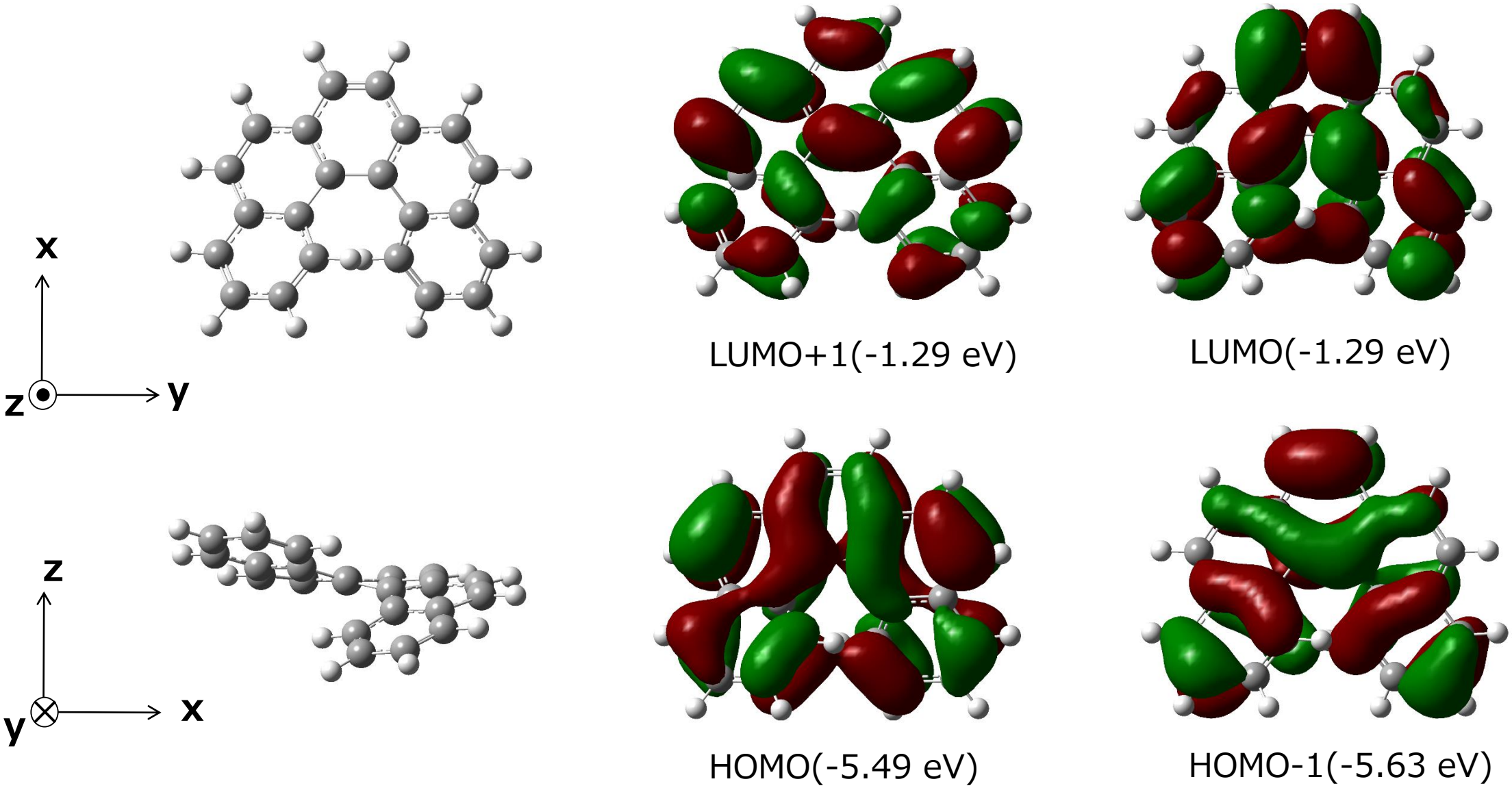

Figure S12 Molecular orbitals of [5]-helicene (5b).

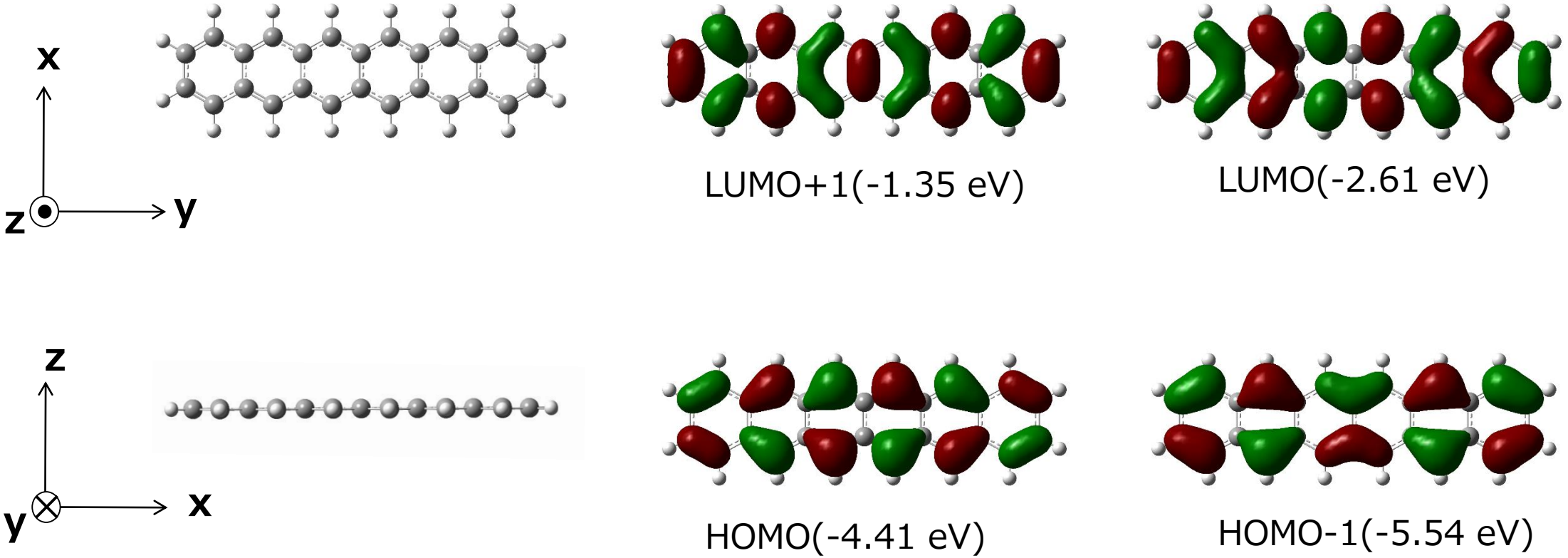

Figure S13 Molecular orbitals of hexacene (6a).

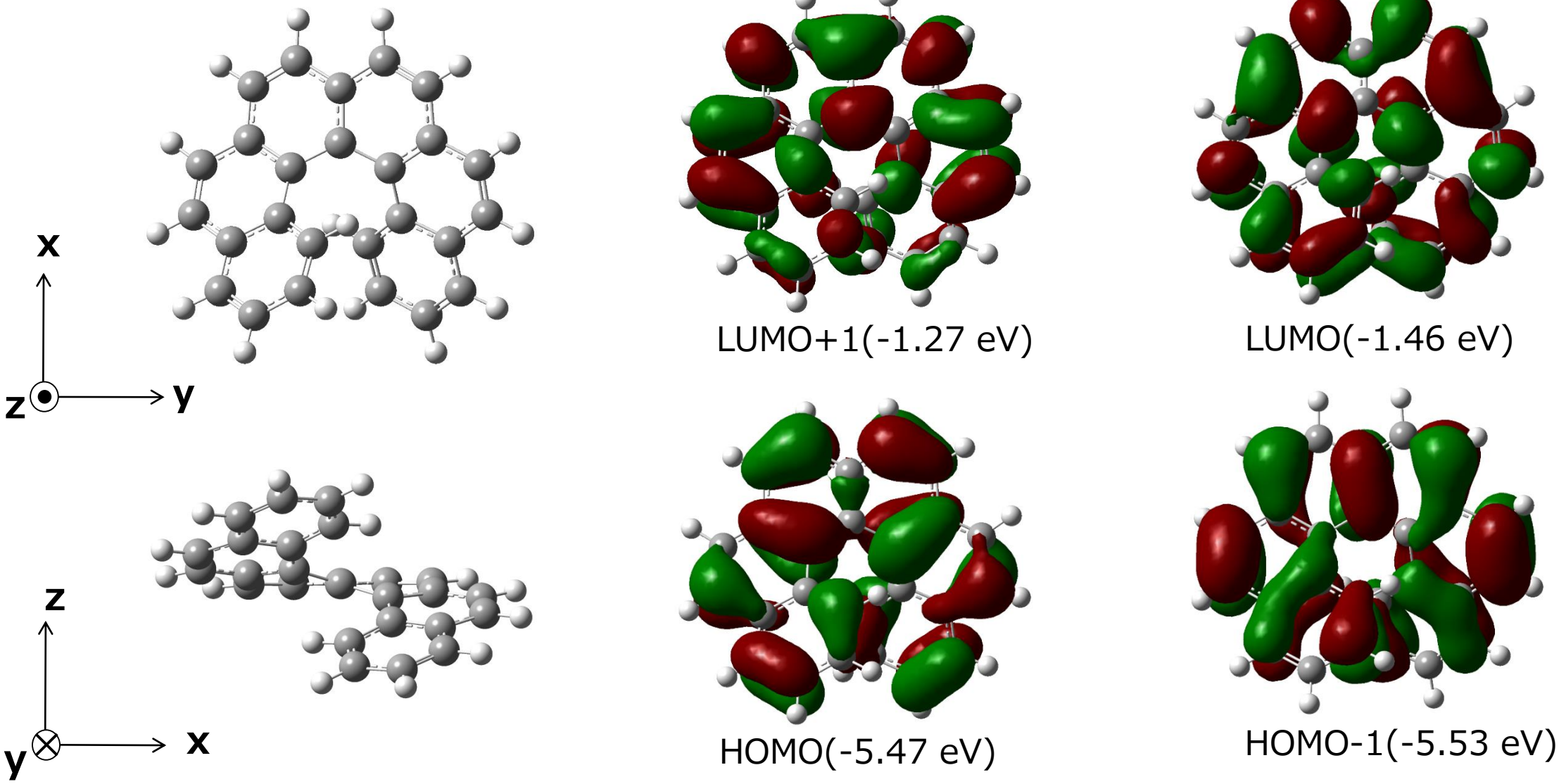

Figure S14 Molecular orbitals of [6]-helicene (6b).

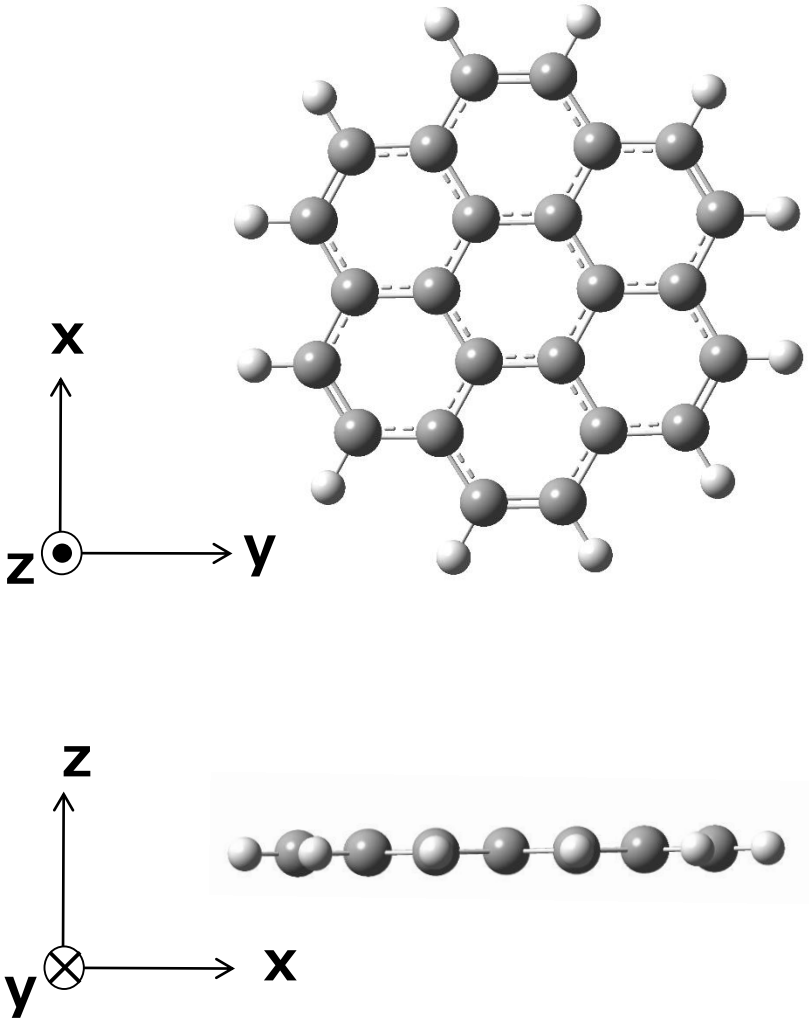

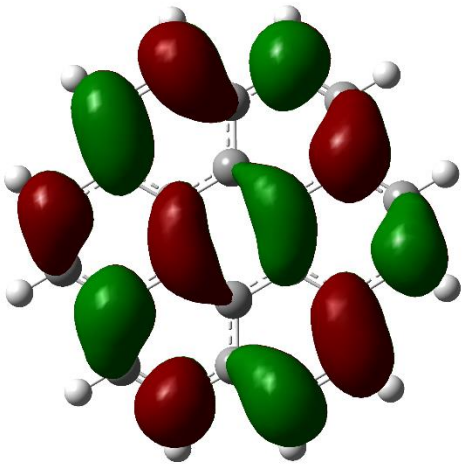

LUMO+1(-1.41 eV)

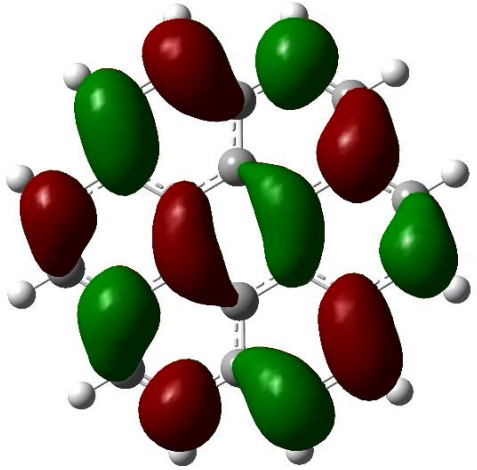

LUMO(-1.41 eV)

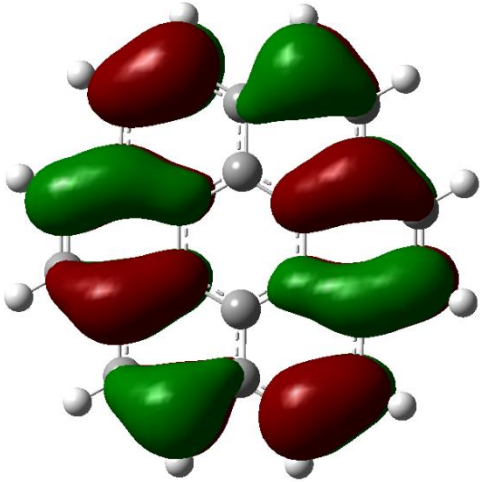

HOMO(-5.45 eV)

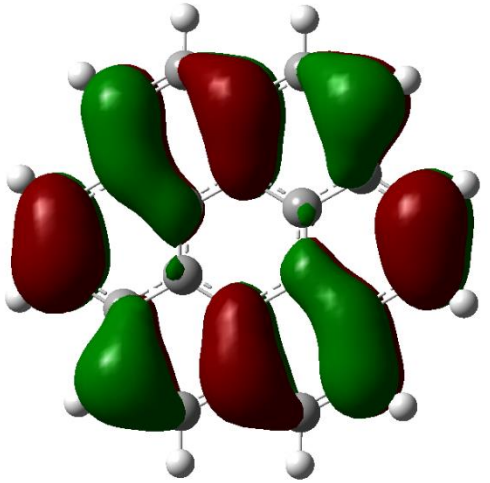

HOMO-1(-5.45 eV)

Figure S15 Molecular orbitals of coronene (6c).

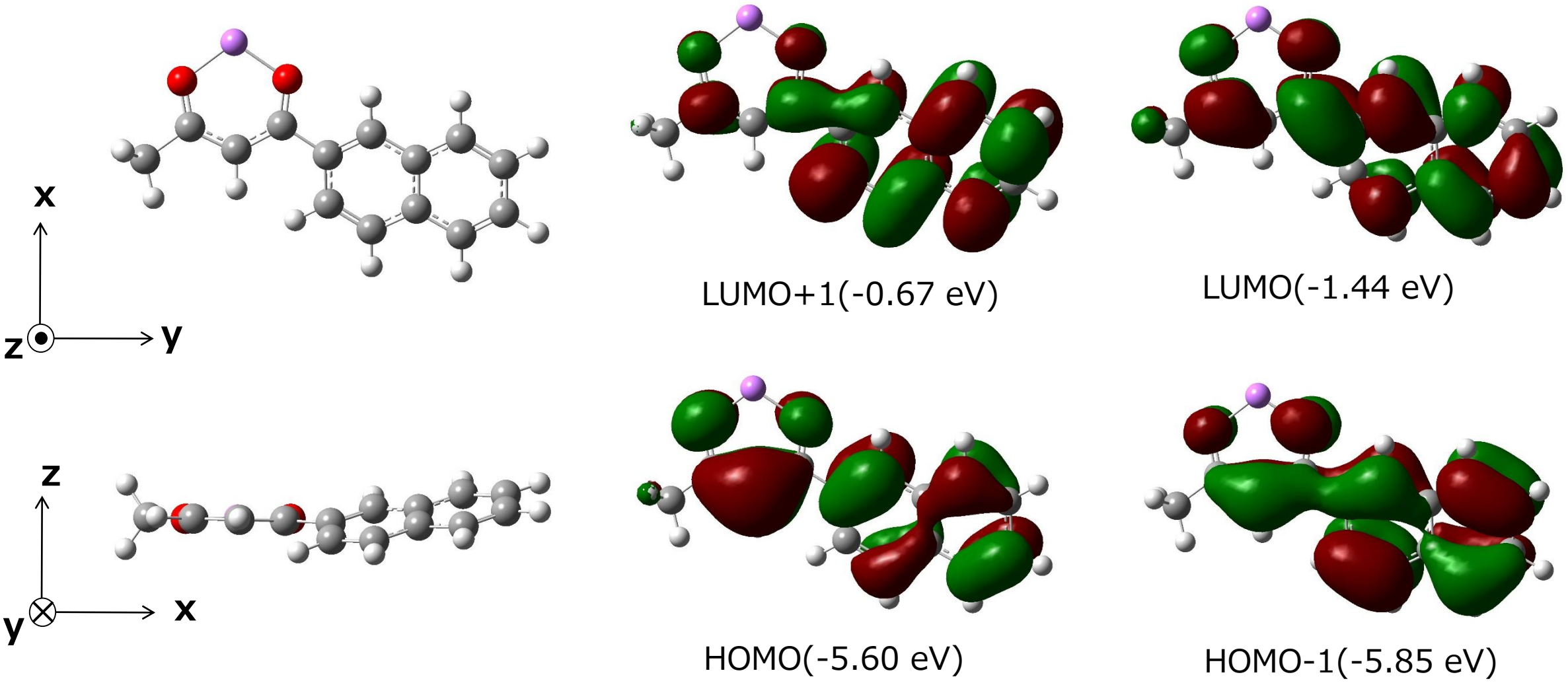

Figure S16 Molecular orbitals of Li(nbd).

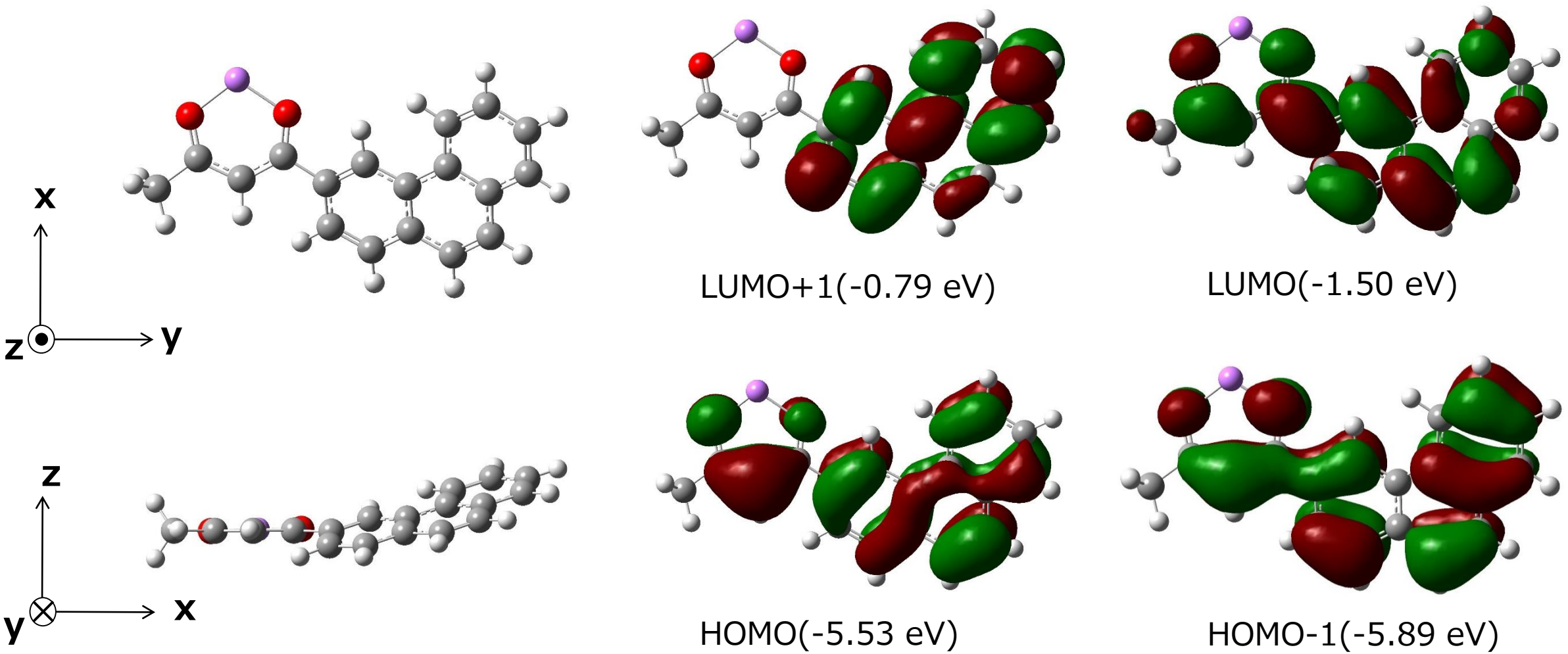

Figure S17 Molecular orbitals of Li(pbd).

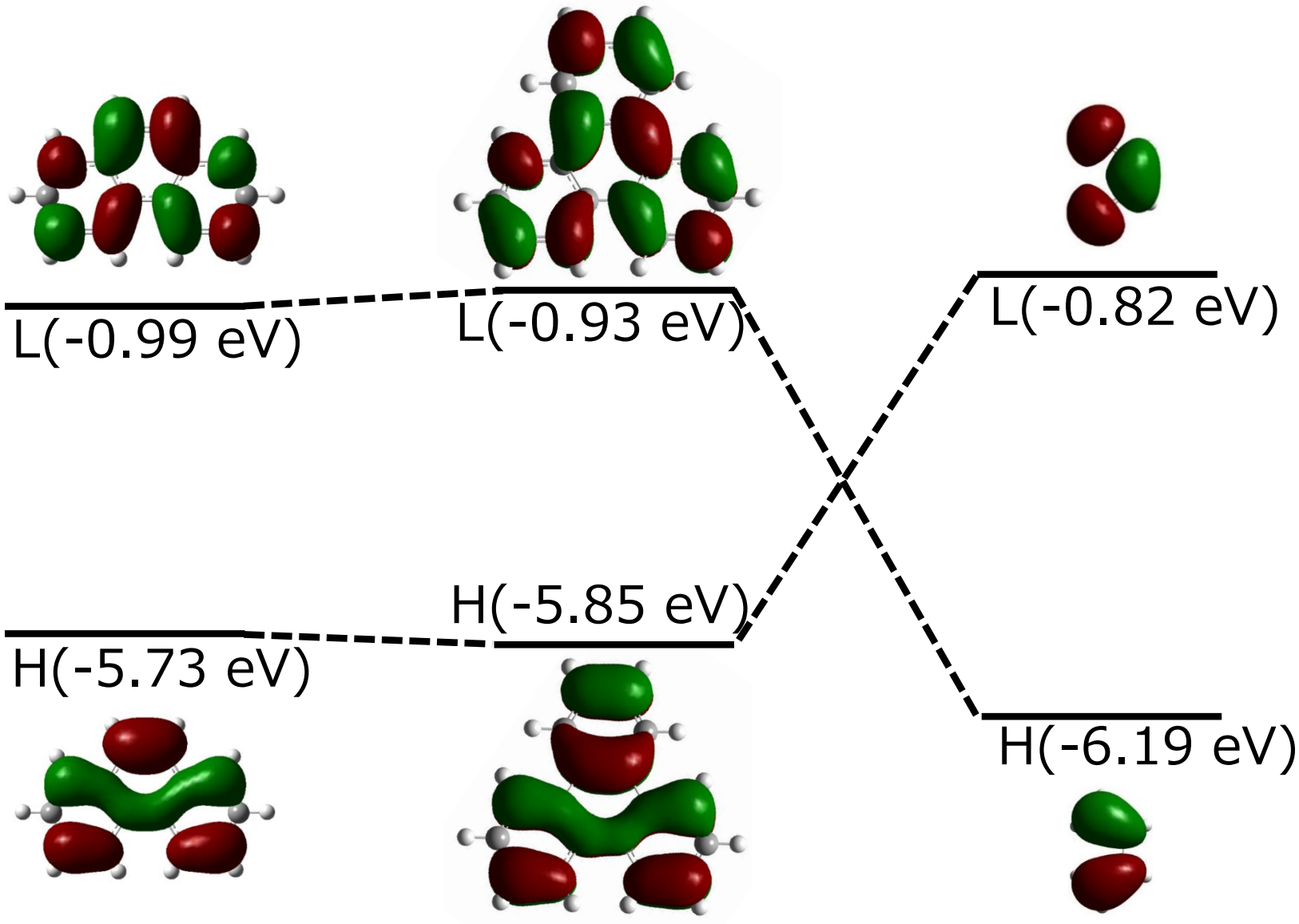

Figure S18 Molecular orbitals of phenanthrene, triphenylene and butadiene.

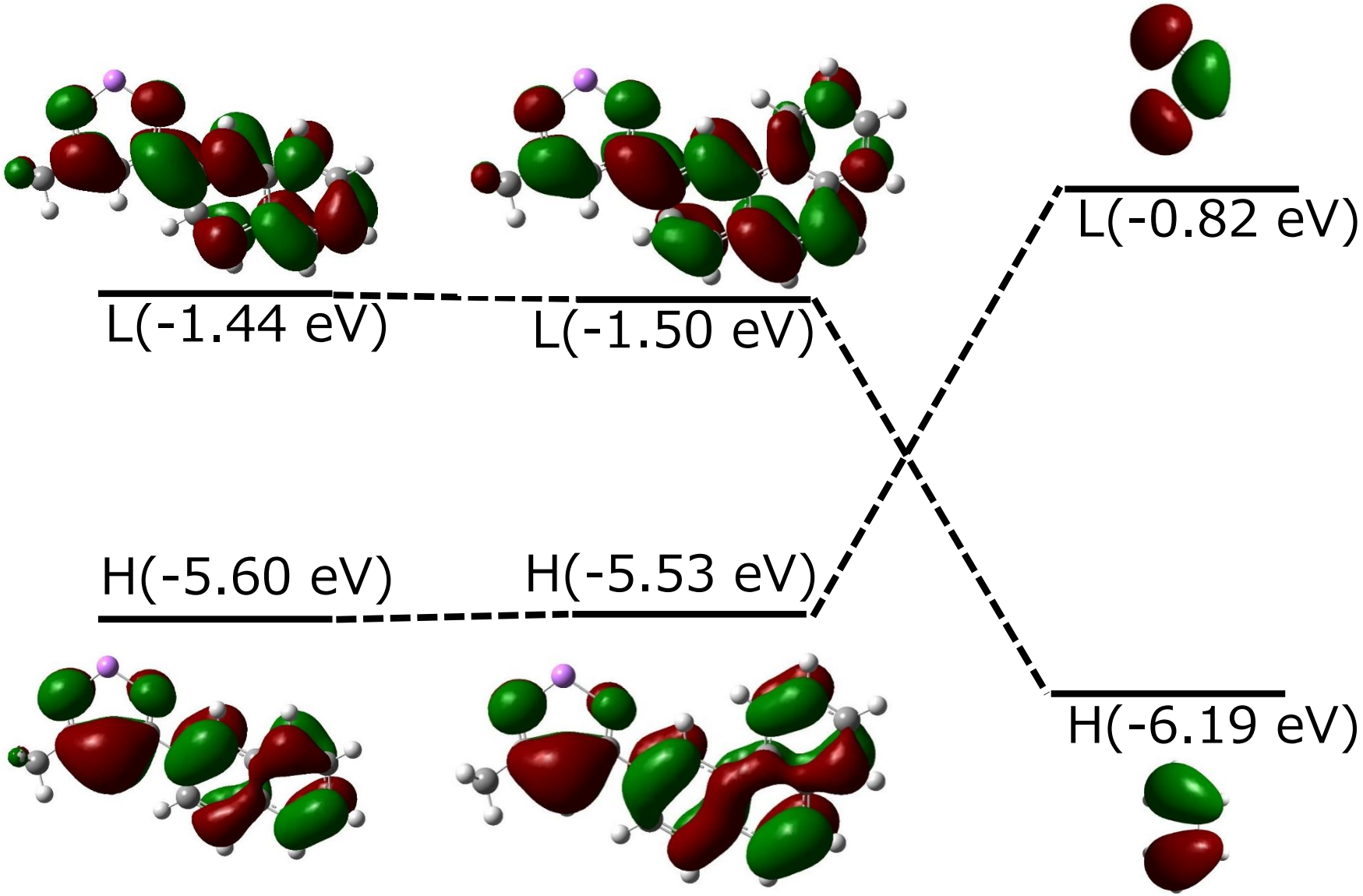

Figure S19 Molecular orbitals of Li(nbd), Li(pbd), and butadiene.

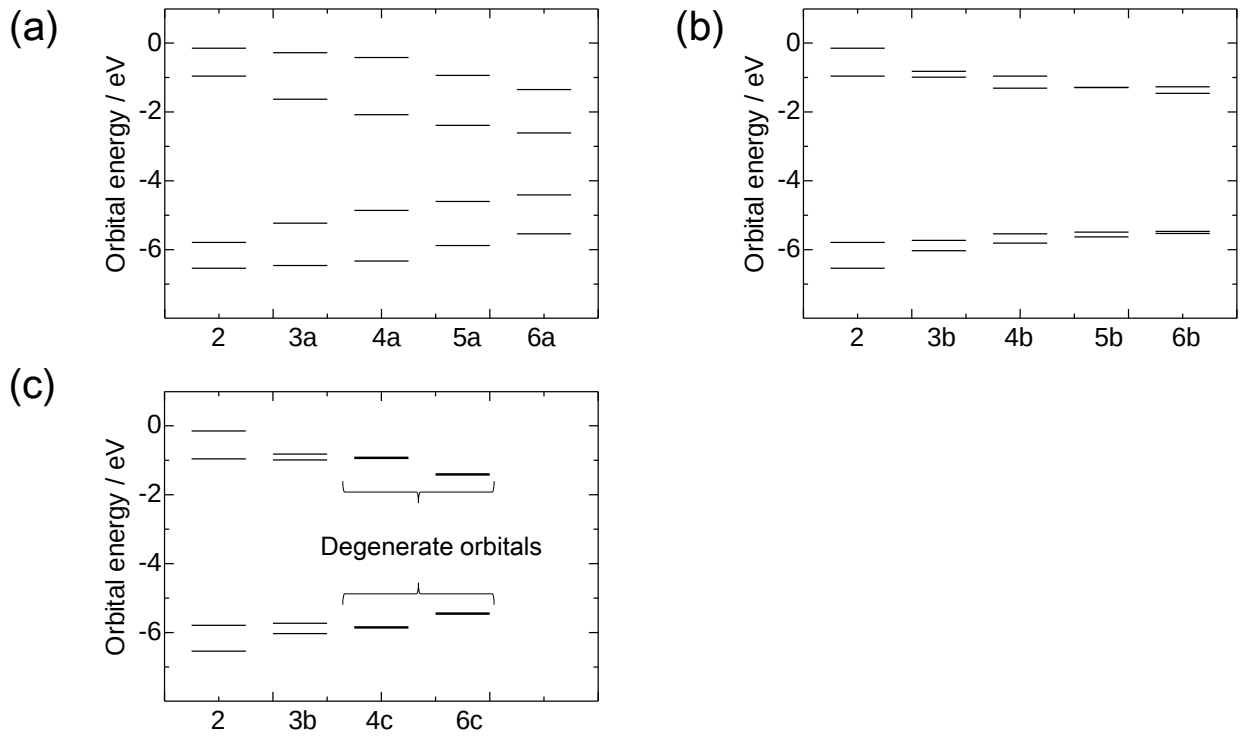

Figure S20. Molecular orbital energy change (a: Naphthalene (2), Anthracene (3a), Tetracene (4a), Pentacene (5a), Hexacene (6a)) (b: Naphthalene (2), Phenanthrene (3b), [4]-helicene (4b), [5]-helicene (5b), [6]-helicene (6b)) (c: Naphthalene (2), Phenanthrene (3b), Triphenylene (4c), Coronene (6c)).